International Journal of Basic and Applied Chemical Sciences ISSN: 2277-2073 (Online)
An Online International Journal Available at http://www.cibtech.org/jcs.htm
2013 Vol. 3 (1) January-March, pp.50-59/ Anjaneyulu et al.
Research Article

STRUCTURAL AND MAGNETIC PROPERTIES OF $CU_{1-X}ZN_XFE_2O_4$ NANO-POWDERS SYNTHESIZED BY OXALATE BASED PRECURSOR METHOD

***Anjaneyulu T.[1], Narayana Murthy P.[2], Narendra K[3] and Vijaya Kumar K[4]**
[1]*Department of Physics, Narasaraopet Engineering College, Narasaraopet - 522 601, A. P., India*
[2]*Department of Physics, Acharya Nagarjuna University, Guntur – 522 510, A. P., India*
[3]*Department of Physics, V.R. Siddhartha Engineering College, Vijayawada - 520 007, A. P., India*
[4]*Department of Physics, JNTUH.College of Engineering, Nachupally, Karimnagar - 505 501, A.P., India*
**Author for Correspondence*

ABSTRACT
Nanocrystalline Cu-Zn ferrites have been synthesized using oxalic based precursor method. Cu-Zn ferrites were formed at very low temperature without any impurities. The particle sizes were observed to decrease from 29 nm to 19 nm with increasing non-magnetic Zn doping. The lattice constant was observed to increase with increasing Zn doping concentration. The observed particle size from the XRD measurements is very well in agreement with SEM analysis. X-ray density was observed to increase with increasing zinc content *x*. The bond lengths were observed to increase with increasing Zn content. The saturation magnetization initially increases with increasing zinc content and reaches a maximum and then decreases. The increase in saturation magnetization may be attributed to the fact that, small amount of Zn ions substituted for Cu occupy A sites displaces Fe ions from A sites to B sites, which increases the content of Fe ions in B sites. This leads to an increase of magnetic moment in B-site and a decrease of magnetic moment in A-site. The reduction in A-B interaction and an increase of B-B interaction which causes the magnetization to decrease with further increase in Zn content.

Key Words: *Nanoferrites, Cu-Zn ferrite, Structural properties, Magnetic properties*

INTRODUCTION
Ferrites are an important class of materials that have potential applications in integrated circuitry, transformer cores, magnetic recording etc (Suzuki, 2001 and Sugimoto, 1999). Ferrite nanoparticles have the potential to replace bulky external magnets in current devices. The study of ferrite nanoparticles is of interest due to the fundamental differences in their magnetic and electronic properties compared to the bulk counterparts (Tanaka, 1999). Copper zinc ferrites crystallize in cubic spinel structure. The Cu-Zn ferrites nanoparticles properties can be influenced by several factors such as the chemical composition, electronic configuration, ionic radius, synthesis techniques etc (Smit and Wijn, 1959).
Nanocrystalline Cu-Zn ferrite have been extensively investigated due to their potential applications in non-resonant device, radio frequency circuits, rod antennas, high quality filters, transformer cores, read/write heads for high speed digital tapes and operating devices (Pradan *et al.*, 2008; Lamani *et al.*, 2009). Copper ferrite ($CuFe_2O_4$) is an interesting material and has been widely used for various applications, such as catalysts for environment (Tsoncheva *et al.*, 2010) gas sensor (Tao *et al.*, 2000) and hydrogen production (Faungnawakij *et al.*, 2007). Magnetic and electrical properties of Cu ferrites vary greatly with the change chemical component and cation distribution. For instance, most of bulk $CuFe_2O_4$ has an inverse spinel structure, with 85% Cu^{2+} occupying B sites (Zuo *et al.*, 2006), whereas $ZnFe_2O_4$ is usually assumed to be a completely normal spinel and Zn^{2+} ions preferentially occupy A sites while Fe^{3+} ions would be displaced from A sites for B sites (Yao *et al.*, 2007). Zn-substitution results to a change of cations in chemical composition and a different distribution of cations between A and B sites. Consequently the magnetic and electrical properties of spinel ferrites will change with changing cation

distribution. However, there are no reports on the synthesis and characterize of Cu-Zn ferrites nanoparticles using oxalic acid precursor method in the literatures. Therefore, it would be interesting to synthesize Cu-Zn ferrite nanoparticles using oxalic acid based precursor method and to study the structural and magnetic properties.

EXPERIMENTAL PROCEDURES

Nanocrystalline $Cu_{1-x}Zn_xFe_2O_4$ ($0.0 \leq x \leq 0.8$) was prepared by oxalic acid based precursor method (Wickham, 1967 and Raghavender *et al.*, 2011). All of the chemicals were analytical grade. In a typical procedure, the copper hydrate Cu $(NO_3)_2 \cdot 6H_2O$, zinc nitrate hydrate $Zn(NO_3)_2 \cdot 6H_2O$, ferric nitrate nonahydrate $Fe(NO_3)_3 \cdot 9H_2O$wereused as starting materials. Stoichiometric amounts of metal nitrates were dissolved in deionized water to get clear solution. The obtained aqueous solution of metal nitrates was mixed with oxalic acid in a molar ratio ranging from 1:3 to 1:0.15. The mixture solution were moved on to magnetic stirrer and stirred for 2 h at room temperature. The reaction mixtures turned turbid by varying molar ratios 1:3 and 1:2. When the molar ratio was further lowered to 1:1, precursor solution showed different colour shades. The resultant mixtures were evaporated on a hot plate at 150^0C for 2 h. The obtained raw powders were thermally heat treated at 300◦C for 4 h to get the single phase nanocrystalline Cu-Zn ferrites.

The structural characterization of the prepared Cu-Zn ferrite nanopowders was carried out using Philips X-ray diffraction system with Ni filter using Cu –Kα radiation (wave length λ= 1.54 A^o). The average particle size *D* was calculated using most intense peak (311) employing the Scherer formula. The particle size and morphology was carried out using FE-SEM (model JSM-7000F) manufactured by JEOL Ltd. The FE-SEM was linked to an EDS/INCA 350 (energy dispersive X-ray analyzer) manufactured by Oxford Instruments Ltd. The structural changes were observed by ABB Bomem MB 102 infrared spectrometer. The samples were mixed with KBr and made in the form of pellets and recorded at 4 cm^{-1} resolution. Magnetic measurements were performed using Lakeshore VSM 7410 at room temperature with maximal applied magnetic fields of 10 kOe. Maximum magnetization, coercivity and remanent magnetization were observed from the hysteresis loops.

RESULTS AND DISCUSSION

Figure 1 shows the X-ray diffractograms of $Cu_{1-x}Zn_xFe_2O_4$ ($0.0 \leq x \leq 0.8$). The XRD patterns clearly indicate that the prepared samples contain cubic spinel structure only.

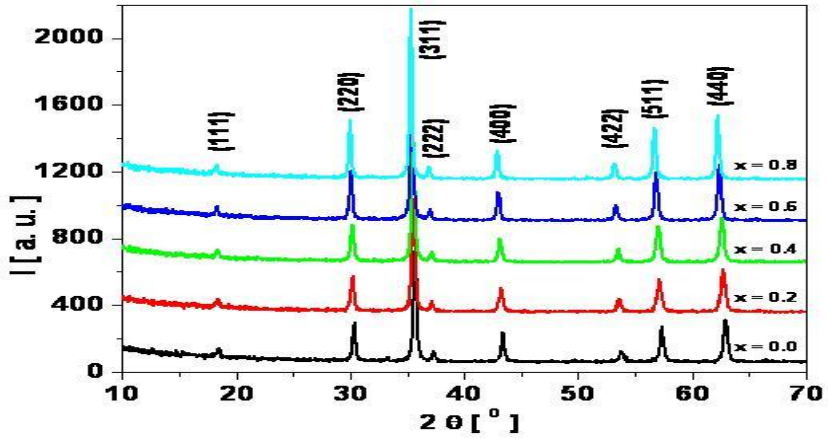

Figure 1: X-ray diffraction pattern of $Cu_{1-x}Zn_xFe_2O_4$ ($0.0 \leq x \leq 0.8$) nanoparticles

From the XRD it can be clearly seen that no secondary phases exists and the prepared ferrite nanopowders contains only single phase spinel structure. A close examination of XRD patterns as shown

in Figure 2 reveals that the diffraction peaks became broader with increasing Zn content *x*, which may be attributed due to the reduced nanocrystallite size with Zn doping.

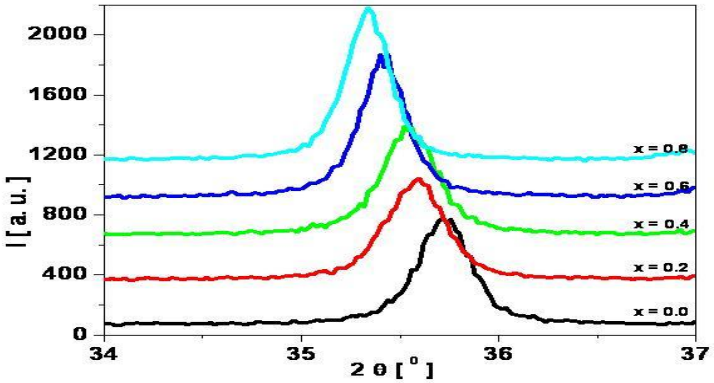

Figure 2: X-ray diffraction pattern of high intensity (311) peak $Cu_{1-x}Zn_xFe_2O_4$ ($0.0 \leq x \leq 0.8$) nanoparticles

It can be clearly observed from Figure 2 that the full-width at half maximum (FWHM) increases upon increasing Zn doping and it results in the decrease of particle size. The probable reason for this kind effect may be due to the reaction time and temperature during the synthesis process. Generally in the case of nano ferrites, behavior such as decrease in the particle with the increase in the doping concentration is seen quite common (Raghavender *et al.*, 2007 and Auzans *et al.*, 1999). The sizes of crystallite size of all the samples is evaluated by measuring the FWHM (Figure 2) of the most intense peak (311) using the Scherer formula (equation 1).

$$D = \frac{0.9\lambda}{\beta \cos\theta} \qquad (1)$$

Where, D is the average crystalline size, λ is the X-ray wavelength, β the angular line width of half maximum intensity and θ is the Bragg angle in degrees.

The observed particle size of $Cu_{1-x}Zn_xFe_2O_4$ ($0.0 \leq x \leq 0.8$) is listed in Table 1. Furthermore, it is observed from Table 1 that, the particle size D decreases with increasing Zn content x and is plotted as shown in the Figure 3.

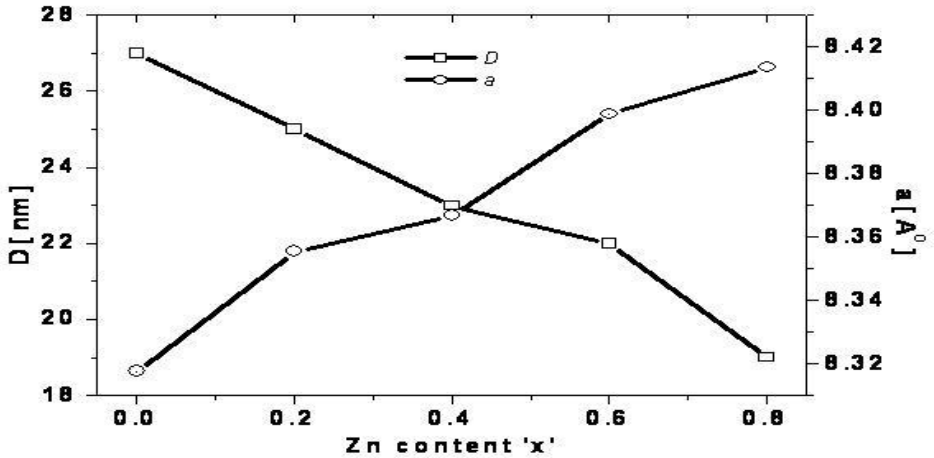

Figure 3: Particle size and lattice values of $Cu_{1-x}Zn_xFe_2O_4$ ($0.0 \leq x \leq 0.8$) nanoparticles

The values for lattice constants were obtained for all the $Cu_{1-x}Zn_xFe_2O_4$ nanoparticles using the most intense (311) peak from XRD data. The values of lattice constants are listed in Table 1 and plotted is as shown in Figure 3. The lattice constant *a* is observed to increase with increasing the non-magnetic Zn content *x*. This behavior of lattice constant with Zn content *x* is explained on the basis of difference in the ionic radii of Cu^{2+} and Zn^{2+}. The $Cu_{1-x}Zn_xFe_2O_4$ system has a cubic spinel configuration with unit cell consisting of eight formula units of the form $(Zn_xFe_{1-x})^{A}[Cu_{1-x}Fe_{1+x}]^{B}O_4$. The Cu^{2+} ions have a preference for the octahedral sites and Zn^{2+} ions have preference for the tetrahedral sites. The observed linear increasing of lattice constant with Zn content *x* can be attributed to the large ionic radius of Zn^{2+} (0.84 A^0) as compared to the ionic radius of Cu^{2+} (0.79 A^0). The larger ionic radii Zn^{2+} atoms replaces the smaller ionic radii Cu^{2+} atoms and thus the lattice parameters shows increasing trend with increasing non-magnetic Zn content in $CuFe_2O_4$. A similar linear variation of lattice constant has been observed by (Patange *et al.*, 2009).

The X-ray density of the $Cu_{1-x}Zn_xFe_2O_4$ nanoferrites samples has been calculated from the molecular weight and the volumes of the unit cell using the equation 2.

$$d_x = \frac{8M}{Na^3}[g/cm^3] \qquad (2)$$

Where, 8 represents the number of molecules in a unit cell of spinel lattice, *M* is molecular weight, *N* is Avogadro's number and *a* is lattice parameter.

Table 1: Particle size *D*, Lattice values *a*, X-ray density d_x of $Cu_{1-x}Zn_xFe_2O_4$ ($0.0 \le x \le 0.8$) nanoparticles

X	D [nm]	a [A^0]	d_x [g / cm^3]
0.0	27	8.318	5.525
0.2	25	8.356	5.548
0.4	26	8.367	5.444
0.6	22	8.399	5.391
0.8	19	8.414	5.371

The values of X-ray density '*dx*' are given in Table 1. It can be seen from Table 1 that X-ray density increases with increasing zinc content *x*. The increase in X-ray density can be related with the lattice constant. In the present series of Cu–Zn spinel ferrites, the lattice constant increases with Zn^{2+} composition *x*. Due to the increase in lattice constant, X-ray density should have been decreased, but in the present case molecular weight increases which overtake the increase in volume of the unit cell and hence X-ray density increases with Zn content *x*.

Table 2: Tetrahedral bond (d_{AX}), octahedral bond (d_{BX}), tetra edge (d_{AXE}) and octa edge (d_{BXE}) (shared and unshared) of $Cu_{1-x}Zn_xFe_2O_4$ ($0.0 \le x \le 0.8$) nanoparticles.

X	d_{AX} (Å)	d_{BX} (Å)	Edges		
			Tetra edge (Å)	Octa edge d_{BXE} (Å)	
			d_{AXE}	Shared	Unshared
0.0	1.887	2.033	3.081	2.799	2.948
0.2	1.896	2.042	3.095	2.812	2.962
0.4	1.898	2.045	3.100	2.816	2.966
0.6	1.906	2.053	3.111	2.826	2.977
0.8	1.909	2.056	3.170	2.831	2.982

The bond length of tetrahedral (A) site d_{Ax} (shortest distance between A-site cation and oxygen ion) and octahedral [B] site d_{Bx} (shortest distance between B-site cation and oxygen ion), tetrahedral edge d_{AXE}, shared octahedral edge d_{BXE} and unshared octahedral edge d_{BXEU} can be calculated by substituting the experimental values of lattice parameter a and oxygen positional parameter u of each sample using equations 3 to 7.

The values calculated from above mentioned equation are presented in Table 2. Table 2 indicate that the tetrahedral bond length d_{AX} and octahedral bond length d_{BX} increases as Zn^{2+} content x increases as shown in Figure 4.

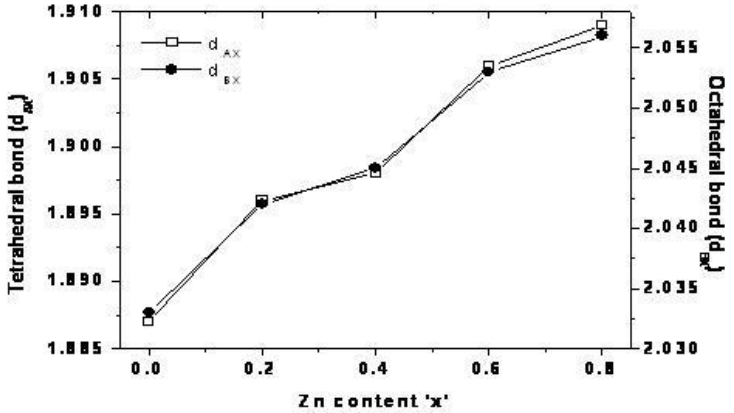

Figure 4: Effect of Tetrahedral bond (d_{AX}), octahedral bond (d_{BX}) on $Cu_{1-x}Zn_xFe_2O_4$ ($0.0 \leq x \leq 0.8$) nanoparticles

The tetrahedral edge d_{AXE}, shared octahedral edge d_{BXE}, unshared octahedral edge d_{BXEU} does not vary much with increasing Zn composition as shown in Figure 5. This could be related to the radius of Ni^{2+}, Zn^{2+} and Fe^{3+} ions.

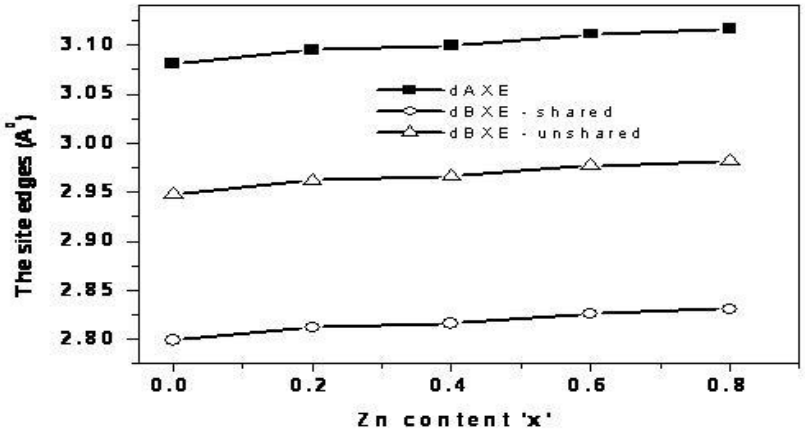

Figure 5: Effect of tetra edge (d_{AXE}) and octa edge (d_{BXE}) (shared and unshared) on $Cu_{1-x}Zn_xFe_2O_4$ ($0.0 \leq x \leq 0.8$) nanoparticles

$$d_{Ax} = \left(u - \frac{1}{4}\right)a\sqrt{3} \qquad (3)$$

$$(d_{BX}) = aX\sqrt{\left(3u^2 - \frac{11}{4}u + \frac{43}{64}\right)} \quad (4)$$

$$d_{AE} = (2u - \frac{1}{2})a\sqrt{2} \quad (5)$$

$$(d_{BE})_{shared} = (1 - 2u)a\sqrt{2} \quad (6)$$

$$(d_{BE})_{unshared} = aX\sqrt{\left(4u^2 - 3u + \frac{11}{16}\right)} \quad (7)$$

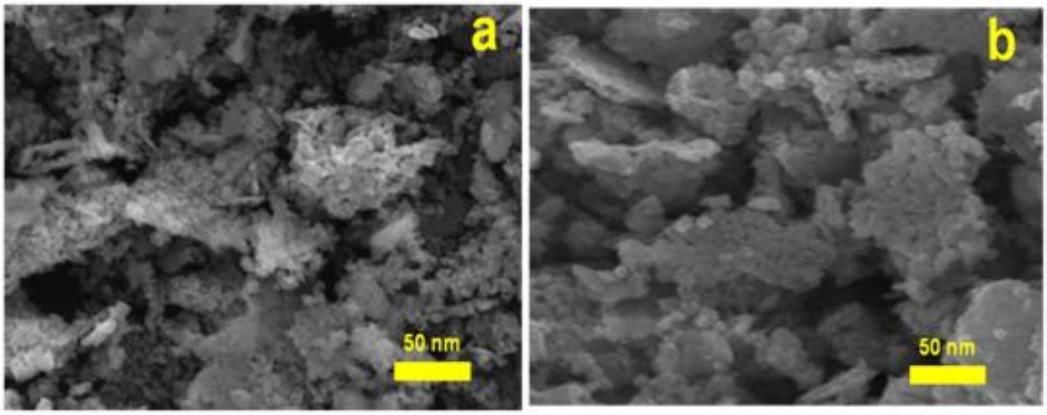

Figure 6: SEM images of $Cu_{1-x}Zn_xFe_2O_4$ (a) x = 0.0 and (b) x = 0.8 nanoparticles

Figure 6 shows SEM images of typical $Cu_{1-x}Zn_xFe_2O_4$ (x = 0.0 and 0.8) nanoparticles. As can be seen in Fig. 6(a) and (b), the microstructure of Cu Zn ferrite is homogeneous. The microstructures of the substituted Ni Zn ferrites depicted in Figure 6(a) reveal a virtually uniform grain size and a homogeneous morphology. According to these micrographs, the microstructure is mainly influenced by the Zn substitution in Cu ferrite. It is observed that porosity affects the magnetic properties of the prepared nano ferrites. The particles are equally distributed and the measurement of particle size is clear. Therefore the observed particle size from the XRD measurements is very well in agreement with SEM analysis.

MAGNETIC PROPERTIES

Hysteresis loops for zinc substituting $CuFe_2O_4$ nanoferrites at room temperature are shown in Figure 7. The values of saturation magnetization (M_s), coercivity (H_c) and remanence (M_r) are given in Table 3.

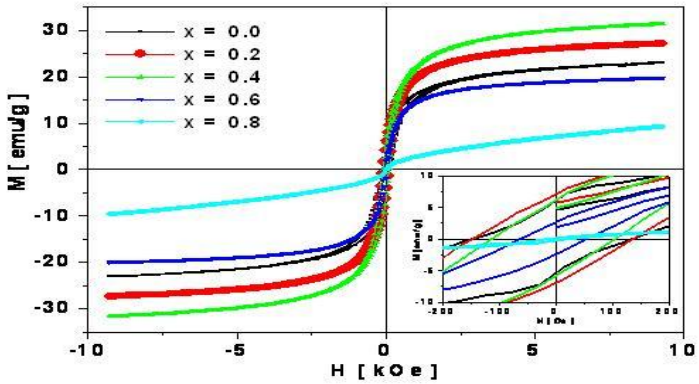

Figure 7: Hysteresis curves for the samples $Cu_{1-x}Zn_xFe_2O_4$ ($0.0 \leq x \leq 0.8$) nanoparticles

Table 3: Coercivity H_c, remanence magnetization M_r, maximum magnetization at M, for $jCu_{1-x}Zn_xFe_2O_4$ ($0.0 \leq x \leq 0.8$) nanoparticles

x	H_c [Oe]	M_r [emu/g]	M_s [emu/g]
0.0	146	5.7	23.2
0.2	141	7.1	27.5
0.4	108	5.9	31.5
0.6	61	2.5	20.1
0.8	15	0.2	9.6

The magnetic properties of Cu-Zn nanoferrites vary with changing zinc content. The variation of magnetic properties of $Cu_{1-x}Zn_xFe_2O_4$ nanoferrites can be understood in term of cation distribution and exchange interactions between spinel lattices.

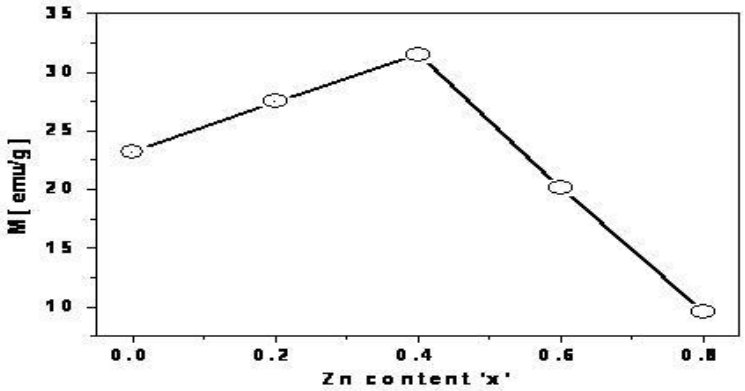

Figure 8: Maximum magnetization values observed for $Cu_{1-x}Zn_xFe_2O_4$ ($0.0 \leq x \leq 0.8$) nanoparticles from hysteresis loops

The $Cu_{1-x}Zn_xFe_2O_4$ nanoferrites with $x \leq 0.6$ exhibit ferromagnetic behavior, whereas for $x = 0.8$ nanoferrites display paramagnetic character with zero coercivity, zero remanence and non-saturated magnetization. The saturation magnetization initially increases with increasing zinc content and reaches a maximum (31.5 emu/g) and then decreases. The increase in saturation magnetization may be attributed to the fact that, small amount of Zn ions substituted for Cu occupy A sites displaces Fe ions from A sites to B sites, which increases the content of Fe ions in B sites. This leads to an increase of magnetic moment in B-site and a decrease of magnetic moment in A-site. So the net magnetization increases, which is consistent with the increase of saturation magnetization. With further increase nonmagnetic Zn ions substitution, the dilution at the A sites increases. This results in the breakdown of the ferromagnetic phase at $x \leq 0.4$. For $Cu_{1-x}Zn_xFe_2O_4$ ($x = 0.6$ and 0.8), the triangular spin arrangement on B-sites is suitable and this causes a reduction in A-B interaction and an increase of B-B interaction. Therefore, the decrease of saturation magnetization can be explained on the basis of three sublattice model (Yafet and Kittle, 1952).
As shown in Table 3, coercivity (H_c) continuously reduced with increasing Zn ions content. These magnetic behaviors of ferrite depends intirely on the spinel structure. For instance, normal spinel ferrite shows an antiferromagnetically ordering, while inverse spinel ferrite shows a ferromagnetic ordering. With increasing Zn ions concentration, a transformation from inverse spinel structure of $CuFe_2O_4$ ferrite to normal spinel structure of $ZnFe_2O_4$ ferrite will arises gradually.
Variation of saturation magnetization with Zn content is as shown in Figure 8. The observed variations can be explained on the basis of cations distribution and exchange interaction between Fe ions and between Zn ions at the tetrahedral A and octahedral B sites. When Zn ions are introduced at the expense of Cu ions, some of the Fe ions migrate from A – to the B- sites. This increases the Fe ion concentration

at B-sites. As a result, the magnetic moment of B sub-lattices increases with increasing Zn concentration up to x≤ 0.4. However, as Zn concentration increases, the Fe ions left at A-site being small in number, the A–B interaction experienced by B-site iron ions decreases. Also, the increased number of Fe ions at the B-site increases the B–B interaction, resulting in spin canting (Kakatkar *et al.,* 1996). The decrease in the B sub-lattice moment, interpreted as a spin departure from co-linearity, causes the effect known as canting. Magnetization values for the present Cu-Zn nanoferrites were observed to be smaller than that of ceramically prepared samples (Sattar *et al.,* 2005). This might be due to several reasons such as Nanocrystalline nature, surface disorder, modified cationic distribution etc. (Parvatheeswara Rao *et al.,* 2007).

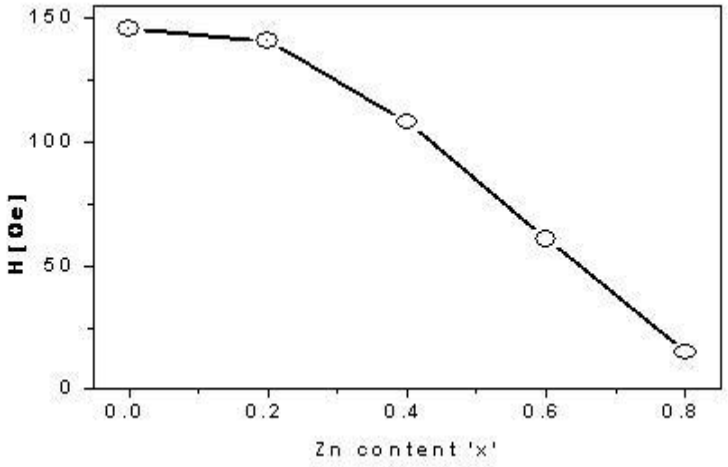

Figure 9: Coercivity (H_c) values observed for $Cu_{1-x}Zn_xFe_2O_4$ ($0.0 \leq x \leq 0.8$) nanoparticles

Figure 9 shows the change in the coercive force (H_c) with Zn ion concentration. The coercivity is influenced by factors such as magnetocrystalline anisotropy, micro-strain, magnetic particle morphology, size distribution, shape anisotropy, and magnetic domain size. The magnitude of H_c decreases with increase in Zn content. This behavior is similar to that of porosity. Porosity affects magnetization process because pores work as a generator of demagnetizing field. As the porosity decreases high field is needed to push the domain wall and thus Hc decreases.

It is known that the coercive force has a direct relation with the anisotropy constant of the sample, and, according to the one ion model, the anisotropy field of ferrites depends on the amount of Fe ions in the sample (Chikazumi and charap, 1964; Coey, 1996). In the present study, it seems that the amount of Cu^{2+} ions decreases as a result of increase in Zn^{2+} content. This means that the magneto anisotropy constant decreases with increase in Zn content and that, consequently, the magnitude of H_c also decreases. The observed magnetic properties of Cu-Zn nanoferrites were due to the combined effect of reduced particle size as well as with the increase of non-magnetic Zn content.

Conclusion

A series of $Cu_{1-x}Zn_xFe_2O_4$ ($0.0 \leq x \leq 0.8$) nanoparticles were prepared using oxalic acid based precursor method.

The XRD analysis reveals the formation of single phase spinel structure at very low annealing temperature without any secondary phases.

The particle size was observed to decrease with increasing Zn concentration probably due to the reaction temperature and time.

The lattice parameters were observed to increase with increasing Zn content *x,* which is due to large ionic radii of zinc when compared to copper ions.

Magnetic measurements at room temperature for these samples revealed that magnetization at ≈1*T* do not change monotonically with the change of Zn content *x*.
The coercivity and remanence decreases with increasing non-magnetic Zn content *x*.

REFERENCES

Ashok RL, Jayanna HS, Parameshwara P and Somasekhar R (2009). Microcrystalline parameters of Cu-Zn ferrites using X-ray line profile analysis. *Indian Journal of Pure and Applied Physics* **47**(10) 715-719.
Auzans E, Zins D, Blums E and Massart R (1999). Synthesis and properties of Mn-Zn ferrite ferrofluids. *Journal Material Science* **34** 1253-1260.
Chikazumi S and Charap S (1964). *Physics of Magnetism*. John Wiley and Sons, New York, pp.140.
Coey JMD (1996). *Rare Earth Permanent Magnetism* John Wiley and Sons, 1st edition New York 220.
Faungnawakij K, Tanaka Y, Shimoda N, Fukunaga T, Kikuchi R and Eguchi K (2007). Hydrogen production from dimethyl ether stem reforming over composite catalyst of copper ferrite spinel and alumina. *Applied Catalysis* **B74** 144-151.
Kakatkar SV, Kakatkar SS, Patil RS, Sankpal AM, Suryawanshi SS, Bhosale DN and Sawant SR (1996). X-ray and bulk magnetic properties of the Ni-Zn ferrite system. *Physica Status Solidi* **B198** 853-860.
Parvatheeswara Rao B, Caltun O, Cho WS, Chong-Oh Kim and CheolGi Kim (2007). Synthesis and characterization of mixed ferrite nanoparticles. *Journal of Magnetism and Magnetic Materials* **310** e812-e814.
Patange SM, Shirsath Sagar E, Toksha BG, Jadhav SS, Shukla SJ and Jadhav KM (2009). Cation distribution by rietveld, spectral and magnetic studies of chromium-substituted nickel ferrites. *Applied Physica* **A95**(2) 429–434
Pradhan SK, Bid S, Gateshki M and Petkov V (2005). Microstructure characterization and cation distribution of nanocrystalline magnesium ferrite prepared by ball milling. *Materials Chemistry and Physics* **93** 224-230.
Raghavender AT, Pajic D, Zadro K, Milekovic T, Venkateshwar Rao P, Jadhav KM and Ravinder D (2007). Synthesis and magnetic properties of $NiFe_{2-x}Al_xO_4$ nanoparticles. *Journal of Magnetism and Magnetic Materials* **316** 1-7.
Raghavender AT, Shirsath SE and Vijaya Kumar K (2011). Synthesis and study of nanocrystalline Ni-Cu-Zn ferrites prepared by oxalate based precursor method. *Journal of Alloys and Compounds* **509**(25) 7004-7008.
Sattar AA, El-Sayed HM, El-Shokrofy KM and El-Tabey MM (2005). Effect of manganese substitution on the magnetic properties of nickel-zinc ferrite. *Journal of Materials Engineering and Performance* **14**(1) 99-103.
Smit J and Wijn HPJ (1959). *Ferrites* _Philips Technical Library, Eindhoven.
Sugimoto M (1999). The past, present and future of ferrites. *Journal of the American Ceramic Society* **82** 269-280.
Suzuki Y (2001). Epitaxial spinel ferrite thin films. *Annual Review of Material Research* **31** 265-289.
Tanaka T (1999). Nonequilibrium strain and curie temperature in as-deposited Mn ferrite thin films by RF sputtering. *IEEE Transactions on Magnetics* **35** 3010-3012.
Tao SW, Gao F, Liu XQ and Sørensen OT (2000). Preparation and gas-sensing properties of $CuFe_2O_4$ at reduced temperaure. *Materials Science and Engineering* **B77**(2) 172-176.
Tsoncheva T, Manova E, Velinov N, Paneva D, Popova M and Kunev B (2010). Thermally synthesized nanosized copper ferrites as catalysts fro environment protection. *Catalysis Communications* **12**(2) 105-109.
Wickham DG (1967). *Inorganic Synthesis* **9** 152.

Yafet Y and Kittel C (1952). Antiferromagnetic arrangements in ferrites. *Physical Review* **87** 290-294.
Yao CW, Zeng QS, Goya GF, Torres T, Liu JF and Jiang JZ (2007). $ZnFe_2O_4$ nanocrystals: synthesis and magnetic properties. *Journal of Physical Chemistry* **C111** 12274-12278.
Zuo X, Yang A, Vittoria C and Harris VG (2006). Computational study of copper ferrite ($CuFe_2O_4$). *Journal of Applied Physics* **99** 08M909.